Molecular engineering of PEDOT:PSS for enhancing open-circuit voltage in organic/silicon heterojunction solar cells

View Online   Export Citation   CrossMark

Leiming Yu, Rui Yang, (iD) Xiangdong Duan, Zhuo Wu, (iD) Suicai Zhang,[a] Xiaohui Song, (iD) Yurong Jiang, and Congxin Xia[a] (iD)

AFFILIATIONS

School of Physics, Henan Key Laboratory of Advanced Semiconductor & Functional Device Integration, Henan Normal University, Xinxiang 453007, China

[a] Authors to whom correspondence should be addressed: zhangsuicai@htu.edu.cn and xiacongxin@htu.edu.cn

ABSTRACT

Poly(3,4-ethylenedioxythiophene):poly(styrenesulfonate) (PEDOT:PSS)/silicon (Si) heterojunction solar cells (HSCs) have garnered extensive interest owing to their potential for high efficiency and low cost. However, their performance is constrained by a limited open-circuit voltage (V_{OC}). In this manuscript, PEDOT:PSS films endowed with both high conductance and high work function via an alcohol-doping-based molecular engineering strategy were applied to induce strong inversion layers on the n-Si surface and generate large built-in voltage in HSCs. This molecular engineering strategy enables precise modulation of PEDOT:PSS molecular building blocks, achieving a work function tuning range from 4.81 to 4.93 eV while retaining high conductivity exceeding 650 S/cm. A photovoltaic device with alcohol-doped PEDOT:PSS delivers a large V_{OC} of 0.66 V without additional modifications and a power conversion efficiency of 12.80%. This study on the molecular engineering of PEDOT:PSS establishes an effective and simplified pathway for fabricating PEDOT:PSS/Si HSCs with high V_{OC}.

Among various organic materials, the conjugated polymer poly(3,4-ethylenedioxythiophene):poly(styrene sulfonate) (PEDOT:PSS) has become a highly competitive candidate and is widely used in silicon/organic heterojunction solar cells, owing to its high conductivity, excellent transparency, promising antireflection properties, commercial availability, and ease of processability.[1–10] The PEDOT:PSS/Si heterojunction, formed by combining PEDOT:PSS with crystalline silicon and designed to replace the traditional homogeneous buried junction in solar cells, can be constructed without high-temperature doping diffusion processing.[11,12] Additionally, PEDOT:PSS/n-Si HSCs based on this heterojunction are usually fabricated through a full-solution approach in the atmosphere, without using an a-Si:H passivation layer (dependent on vacuum technologies such as plasma-enhanced chemical vapor deposition), thus exhibiting a remarkable low-cost advantage.[13,14] Owing to its simple fabrication process and the excellent optoelectronic properties of silicon, the PEDOT:PSS/Si HSCs has become a promising competitor among emerging photovoltaic technologies.[2] Currently, the power conversion efficiencies (PCEs) of PEDOT:PSS/n-Si HSCs have undergone significant improvement and exceeded 18%.[15,16] However, although many silicon surface passivation technologies, back-surface field formation methods, and conformal contact strategies have been used to improve open-circuit voltage (V_{OC}) of these solar cells, the V_{OC} is still below 630 mV under most conditions, which still lags far behind theoretical simulations and crystalline Si solar cells.[17–20] Therefore, how to achieve a high V_{OC} without increasing the complexity of the preparation process is still an obstacle that needs to be conquered.[21–23]

The V_{OC} is fundamentally determined by PEDOT:PSS/n-Si heterojunction quality. The heterojunction quality relies on both the PEDOT:PSS layer itself and its interface with Si.[4,8,22–24] Achieving a higher V_{OC} hinges on optimizing the work function of PEDOT:PSS to maximize the band bending at the silicon interface while maintaining high electrical conductivity for effective charge carrier transport.[25,26] Conventional methods to increase the work function include surface transfer doping and classical doping.[10,27] Among these, surface transfer doping involves coating PEDOT:PSS film with high work function materials. However, the scarcity of suitable materials and the complexity of the fabrication process (such as vacuum evaporation) limit its further development.[28,29] On the contrary, classical doping is realized by doping additives (such as CuPc, Nafion, MoO₃, and V₂O₅) into the PEDOT:PSS precursor solution.[11,21,28,30,31] Nevertheless, this approach

10 January 2026 13:42:30

suffers from low doping efficiency, and high-concentration doping will significantly degrade the optoelectronic properties of the PEDOT:PSS.[32] So far, it is the key issue to find a facile, precise, and effective strategy to adjust the work function without a complex process or damage to the photoelectric properties of the PEDOT:PSS film.

In this paper, we present a straightforward yet effective molecular engineering method that utilizes alcohols with varying reducibility to modify PEDOT:PSS, thereby enhancing the film's conductivity and fine-tuning its work function. As a result, the work function of PEDOT:PSS can be engineered to span from 4.81 to 4.93 eV, while sustaining conductivity above 650 S/cm. PEDOT:PSS/Si photovoltaic device characterization reveals that the elevated work function of PG-modified PEDOT:PSS films induces a robust inversion layer on the Si surface, thereby significantly enhancing the built-in potential and reducing interface recombination. Through the optimization of the PEDOT:PSS/Si heterojunction interface, a record-high V_{OC} of 0.66 V was ultimately achieved.

Figure 1(a) presents the structure of the PEDOT:PSS molecule, which is composed of PEDOT and PSS linked together by electrostatic interaction. In the PEDOT molecule, the proportion of three functional groups—benzene (B) structure and quinoid (Q_1 and Q_2)—determines its conductivity.[33] Figure 1(b) shows the molecular structures of alcohols with different reducibility [propylene glycol (PG), ethylene glycol (EG), and D-sorbitol (D-S)], which are used to regulate the molecular structure of PEDOT:PSS.[34] Figure 1(c) presents schematic diagrams illustrating the tendency of molecular structural transformation under the action of reducing alcohols. As shown in Fig. 1(c), low reducibility alcohols (LRA) preferentially facilitate the transformation of the benzene (B) structure in PEDOT to the Q_2 form, whereas high reducibility alcohols (HRA) direct this conversion toward the Q_1 state. The quinoid structure is widely recognized as the primary contributor to higher conductivity, and it tends to form linear or fibrillary-like morphologies within the film, and the coil-like benzene structure present in the film gives rise to low conductance.[13,35,36] In addition, modification with an alcohol of appropriate reducibility induces the dissociation of PEDOT:PSS and disrupts the original core–shell structure, promoting the formation of more extended PEDOT chains and establishing continuous conductive pathways, as shown in Fig. 1(c).[37–39]

Raman spectroscopy in the wavenumber range of 1340–1600 cm^{-1} was employed to characterize the influence of alcohols on the molecular structure of PEDOT:PSS.[40] As shown in Fig. 1(d), the pristine PEDOT:PSS exhibits three characteristic groups after peak deconvolution: (i) the peak at 1457 cm^{-1} is associated with the benzene conformation (B) with symmetric $C_a=C_b$ (-O) stretching, (ii) the peak at approximately 1405 cm^{-1} is related to an asymmetric quinoid state (Q_1), and (iii) the 1435 cm^{-1} feature corresponds to the quinoid conformation (Q_2) with symmetric C_a-C_b (-O) stretching.[41–43] The electrical properties of PEDOT:PSS films are mainly determined by the proportions of the three components.[44] As shown in the deconvolution results of the Raman spectra [Figs. 1(d), 1(e), and S1], the relative proportions of the B, Q_1, and Q_2 structures undergo a significant change after alcohol modification. The components of the B structure gradually convert to the Q structures. The proportion of the benzene (B) structure in the PEDOT:PSS films with different alcohols modified does not change significantly, ranging from 3% to 5%, but the proportions of the two quinoid structures show distinct differences.

The PG-modified film exhibits the highest Q_2 proportion (65%). Meanwhile, the content of the Q_1 shows a gradual increase with the enhanced reducibility of the alcohols used.

The composition of PEDOT:PSS was analyzed through XPS measurement, as shown in Figs. 1(f), 1(g), and S1. The S 2p core-level spectra exhibit two prominent contributions: one originating from PEDOT on the low binding energy (BE) side and the other deriving from PSS on the high BE side.[45,46] It can be seen that when normalization is performed according to the highest peak of PEDOT, the -S-/SO$_3$H ratio in the alcohol modified films are higher than that in the original film. This suggests a reduction in the PSS component after alcohol modification, which is attributed to its dissociation from PEDOT. The content of PSS components in different alcohol-modified films also varies. This is due to the different redox properties or hydrophilicity of the modified solvent, resulting in different degrees of dissociation of PEDOT:PSS.[37] These Raman and XPS experimental results confirm the hypothesis regarding molecular structural transformation presented in Fig. 1(c).

The surface morphology analysis was performed by scanning electron microscopy (SEM) and atomic force microscopy (AFM). Figure 2(a) shows an original PEDOT:PSS film, in which there is no rearrangement between PEDOT and PSS, and PEDOT:PSS aggregates in a granular structure. In contrast, the morphology of the alcohol-modified PEDOT:PSS films [Figs. 2(b)–2(d)] undergoes drastic changes, revealing a more obvious fibrous structure. The bright fibrous region is the highly conductive PEDOT, while the darker region is the insulating PSS. The results clearly show that alcohol modification leads to a change in the composition of PEDOT:PSS, from a curled shape rich in benzene structure to a fibrous shape rich in quinoid structure,[47] resulting in a slight increase in the root mean square (RMS) roughness of the modified film, as shown in the AFM image in Figs. 2(e)–2(h).

The electrical properties of alcohol-modified PEDOT:PSS films were characterized by van der Pauw–Hall measurements. Figure 3(a) presents the conductivity of PEDOT:PSS films as a function of the doping concentration of alcohols in the PEDOT:PSS precursor solution. The conductivity values of the PEDOT:PSS films increase significantly with the addition of low-concentration alcohols, uniformly reaching a plateau when the alcohol concentration exceeds 5 wt. %. PG, EG, and D-S modified PEDOT:PSS films all exhibit superior conductivity exceeding 650 S/cm. The corresponding carrier concentration and mobility are shown in Figs. 3(b) and 3(c). The D-S modified PEDOT:PSS films exhibit an ultra-high carrier concentration of 10^{21} cm^{-3}, while the PG-modified films demonstrate a high carrier mobility of 5.37 cm^{2}V^{-1}s^{-1}. We speculate that the discrepancy in these electrical properties is primarily attributed to variations in the internal structure of PEDOT:PSS molecules.

To fabricate unetched photovoltaic devices with high sunlight utilization efficiency, an optical model was constructed to simulate the reflection spectra of the solar cell devices. Figure 3(d) presents the optical constants of PEDOT:PSS films with different alcohols doped in the PEDOT:PSS precursor solution. Figure 3(e) shows a reflectance map of semi-finished devices as a function of PEDOT:PSS thickness and incident wavelength. As shown in Fig. 3(e), the reflectivity of the device varies approximately periodically with the thickness of the PEDOT:PSS film. This phenomenon arises from the interference between the reflected light at the PEDOT:PSS/air interface and that at the PEDOT:PSS/Si interface. It can be concluded that the semi-finished
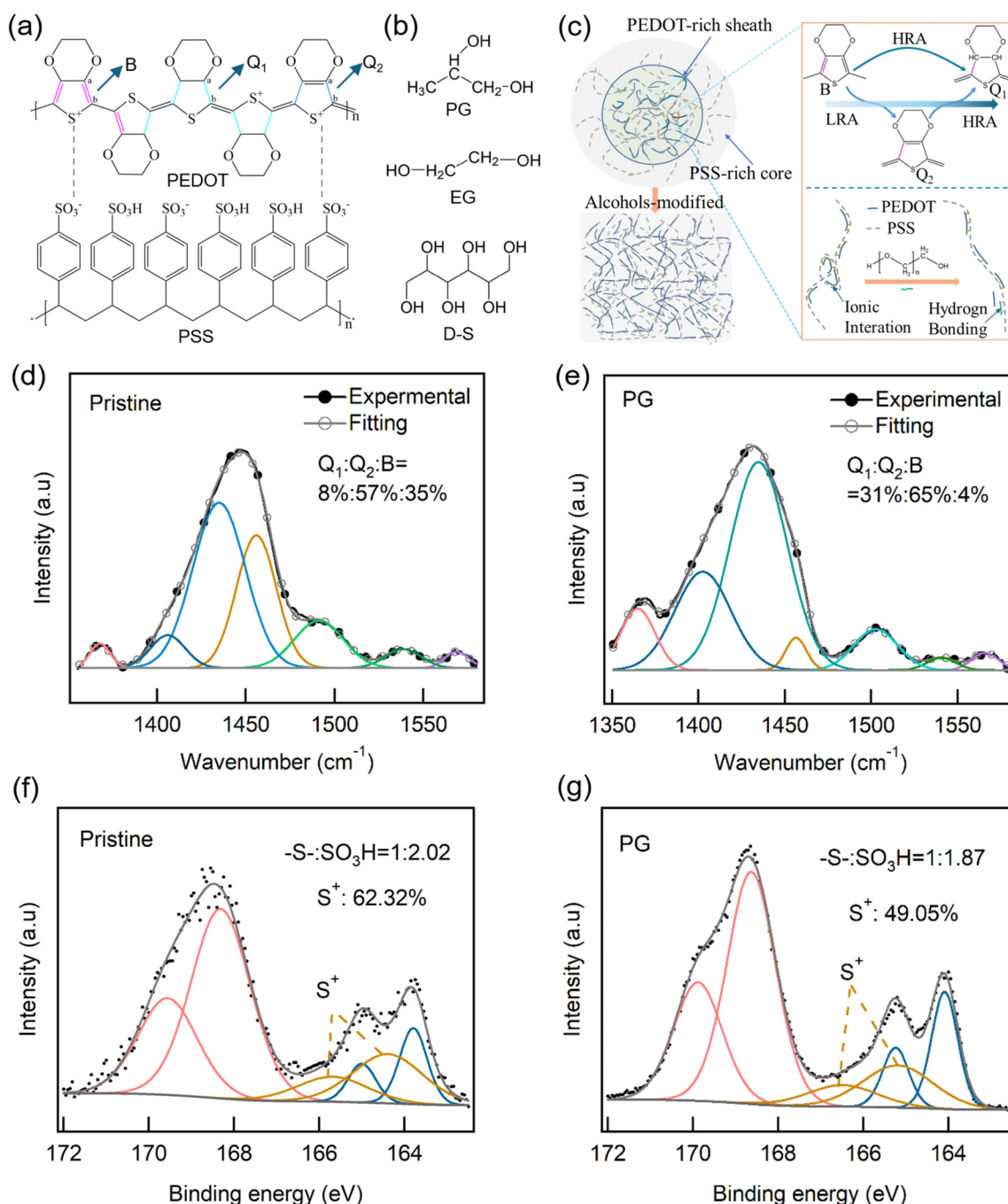
FIG. 1. (a) Schematic structure of PEDOT:PSS. (b) Chemical structures of the different alcohols. (c) Molecular structural schemes of the PEDOT chain (benzene, intermediate, and quinoid forms) illustrating their transformation tendency and the dissociation mechanism of PEDOT:PSS under the action of reducing alcohols. (d) and (e) Peak-fitting analysis of the Raman spectra and [(f) and (g)] XPS spectra of the S 2p core levels for the PEDOT:PSS films.

devices exhibiting the weakest reflectivity should feature a PEDOT:PSS film with a thickness of approximately 90 nm. Figure 3(f) presents the reflection spectra of PEDOT:PSS films modified with different alcohols, with a thickness of approximately 90 nm.

Based on the results of electrical and optical properties characterization, we fabricated PEDOT:PSS/Si HSCs using pristine and three alcohols-modified types of PEDOT:PSS films. Figure 4(a) shows the device configuration of PEDOT:PSS/Si HSCs, which is composed of
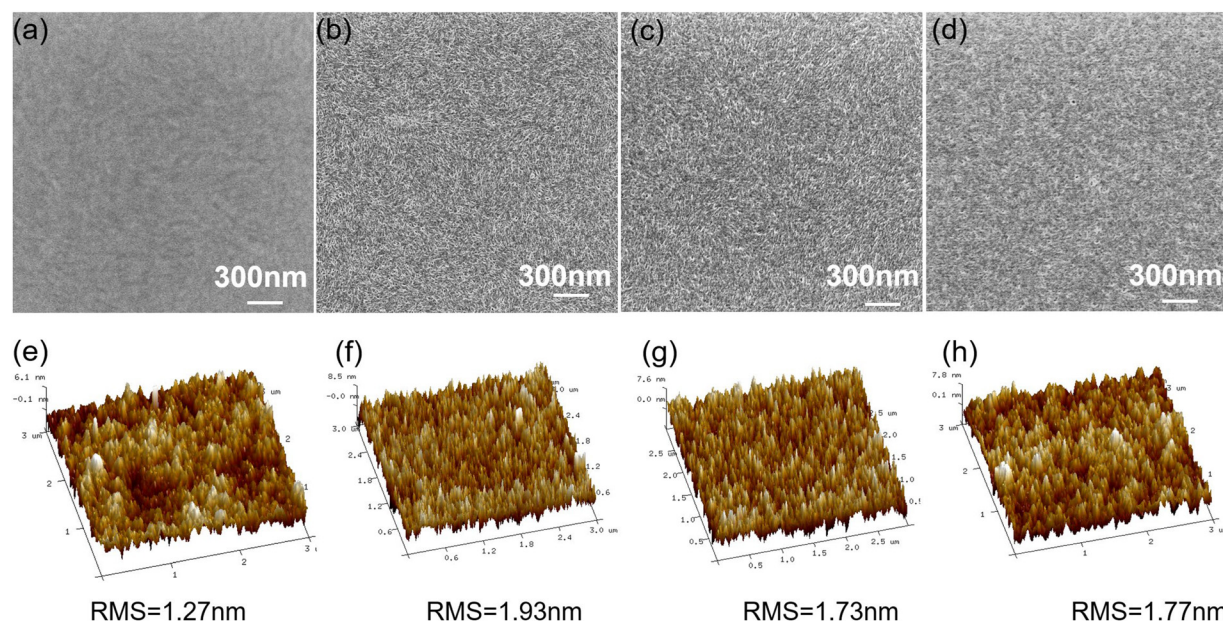
FIG. 2. SEM and AFM images of various PEDOT:PSS films on planar Si substrate: (a) and (e) pristine PEDOT:PSS film; (b) and (f) PEDOT:PSS film with EG doping; (c) and (g) PEDOT:PSS film with PG doping; and (d) and (h) PEDOT:PSS film with D-S doping.

an Ag-grid (200 nm), a PEDOT:PSS film (∼90 nm), an n-type Si wafer (300 μm, 0.05–0.1 Ω·cm), Phenyl-C61-butyric acid methyl ester (PCBM, ∼30 nm), and Al electrode (100 nm). Figure 4(b) shows the J–V characteristic curves of PEDOT:PSS/n-Si HSCs under AM1.5G simulated solar light. For all four types of solar cells, the devices with PG-

modified PEDOT:PSS exhibit the best performance, with a PCE of 12.80% and a V_{OC} of up to 0.66 V (detailed photovoltaic parameters are presented in Table S2). Figure 4(c) presents the dark current density of the corresponding devices. Devices fabricated with PG-modified PEDOT:PSS films exhibit the lowest dark current,
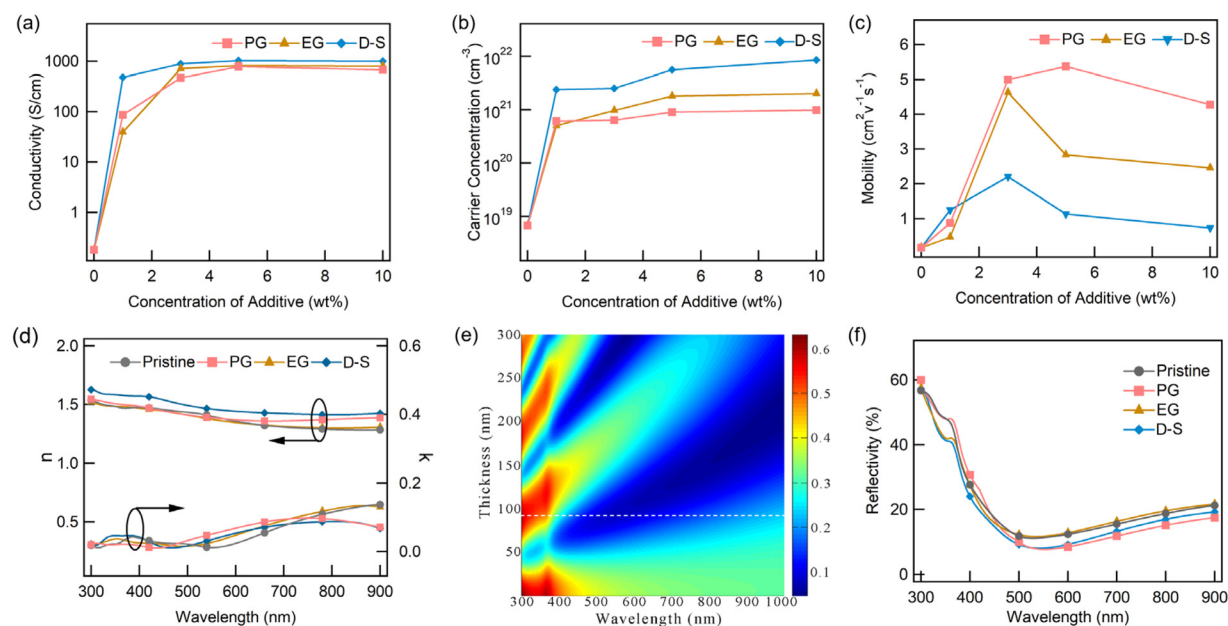

FIG. 3. (a)–(c) Electrical characteristics of PEDOT:PSS films as a function of different alcohol additive concentrations in precursor solution. (d) Optical constants of different alcohol-modified PEDOT:PSS films. (e) Simulated reflectance map of the semi-finished device with pristine PEDOT:PSS film. (f) Experimentally measured reflection spectra of different PEDOT:PSS films.
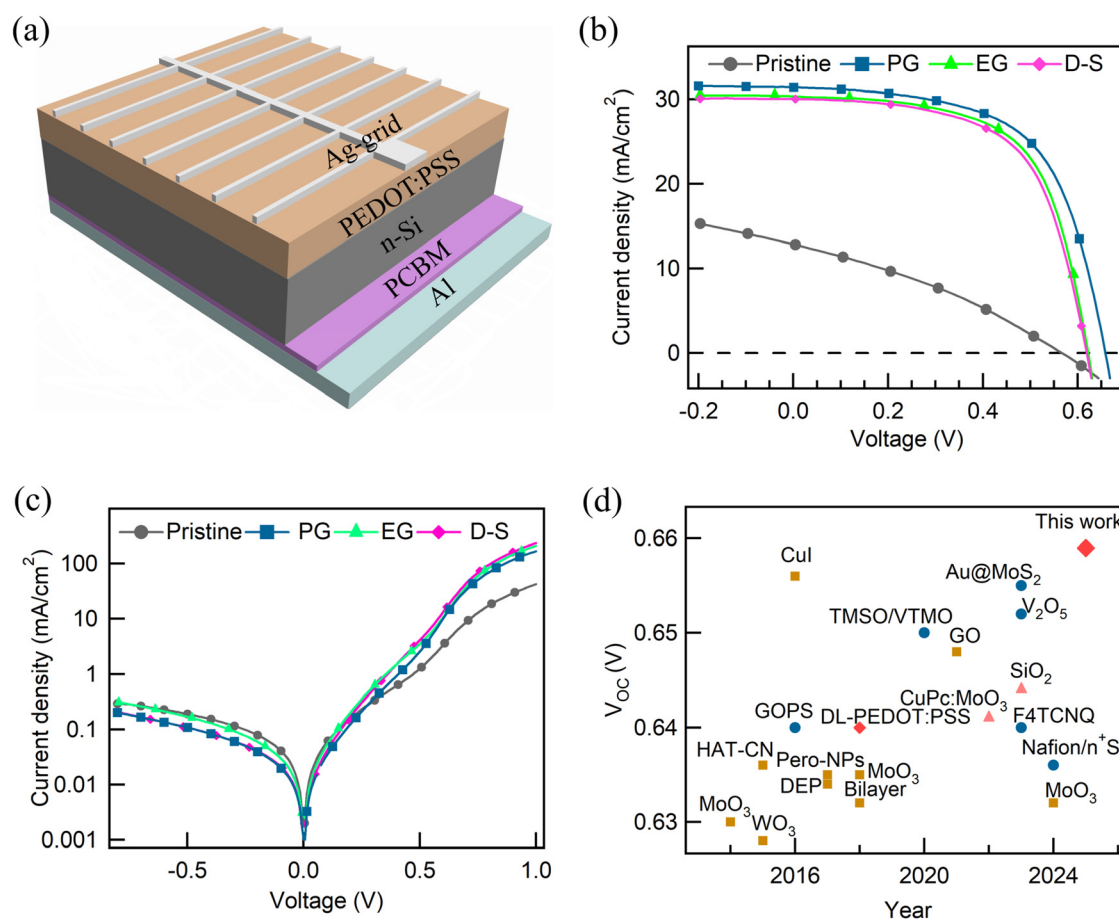
FIG. 4. (a) Schematic illustration of the PEDOT:PSS/Si HSCs structure. (b) The J–V characteristic curves of PEDOT:PSS/Si HSCs with different alcohol-modified PEDOT:PSS films. (c) The dark J–V characteristic curves of the PEDOT:PSS/Si HSCs. (d) The V_{OC} evolution of PEDOT:PSS/Si HSCs over the past 10 years.

indicating that the heterojunction possesses high quality and reduced leakage current. For comparison, Fig. 4(d) summarizes high V_{OC} values reported in the literature over the past decade for PEDOT:PSS/Si HSCs. This confirms the validity of the heterojunction theory and verifies that the band structure of the modified PEDOT:PSS films can serve to enhance the open-circuit voltage of the devices, thereby providing a feasible direction for improving device performance in future research.

The photovoltaic performance results can also be explained by the UPS data and capacitance–voltage (C–V) measurement results. Figure 5(a) shows the UPS spectra of PEDOT:PSS films modified with different alcohols, with molecular structures and compositions shown and discussed above in Fig. 1. The WF of PEDOT:PSS films was adjusted from 4.81 to 4.93 eV. The WF of PEDOT:PSS depends on both the bulk electrochemical potential of electrons within the film and the surface dipole, which is determined by PEDOT:PSS molecular structure and composition.[48,49] The variation in work function among different PEDOT:PSS samples can be ascribed to changes in the internal molecular structure of PEDOT and fluctuations in the PEDOT:PSS ratio. The V_{OC} is related to the magnitude of the built-in electric potential (V_{bi}).[4] C–V measurements were utilized to characterize the

V_{bi} of the HSCs.[24,50,51] The plots of $1/C^2$-V are presented in Fig. S3. The HSCs with PG-modified PEDOT:PSS exhibit a high V_{bi} of 826 mV, which is 75 and 129 mV higher than those of the EG-modified and D-S-modified HSCs, respectively. The improved heterojunction parameters are consistent with the work function values measured by UPS measurements. Figure 5(b) presents the experimentally obtained energy level diagrams of PEDOT:PSS/n-Si contacts. As shown in Fig. 5(b), the PG-modified PEDOT:PSS films have the largest work function, which induces the greatest band bending magnitude and largest V_{OC} in the devices.

In conclusion, we have demonstrated that a simple doping method of PEDOT:PSS with alcohols of varying reducibility can precisely adjust the work function of PEDOT:PSS, which improves the quality of PEDOT:PSS/Si heterojunction. Characterization analysis and device performance reveal that high work function PEDOT:PSS induces a strong inversion layer on the Si surface and forms a high V_{bi} in PEDOT:PSS/Si HSCs. The performance of devices has significantly improved. The champion solar cell, based on PG-modified PEDOT:PSS, exhibits a record V_{OC} of 0.66 V. This thus offers a simple yet effective strategy to further enhance the V_{OC} of organic/silicon heterojunction devices.
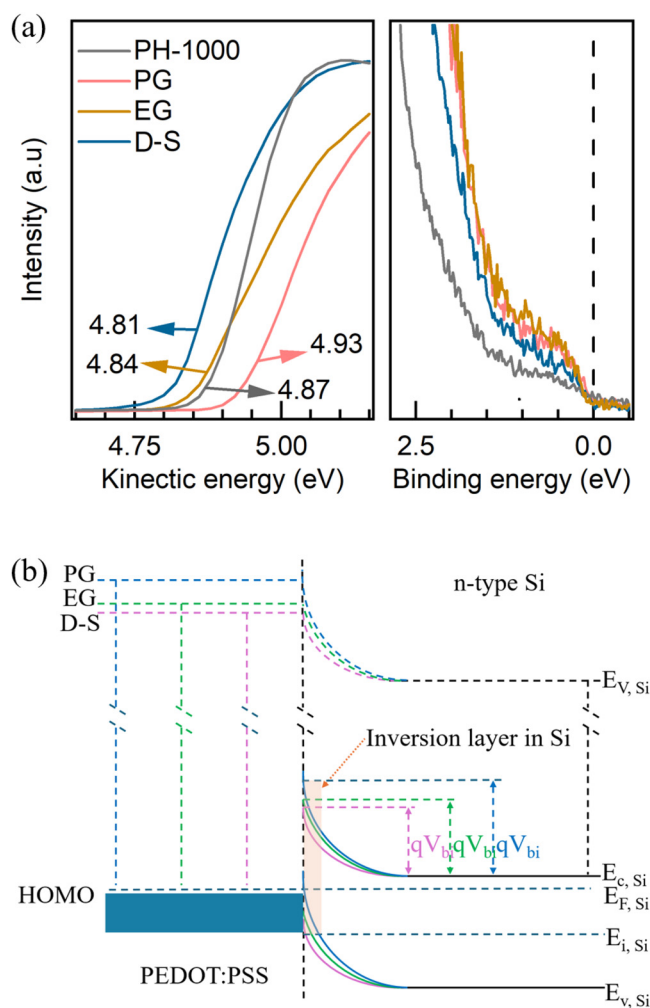
FIG. 5. (a) UPS spectra of alcohol-modified PEDOT:PSS films. (b) Energy band diagrams of PEDOT:PSS/Si heterojunctions derived from UPS spectra.

See the supplementary material for detailed methods of device fabrication, characterization, and measurement, along with supporting data. It includes experimental procedures, additional Raman and XPS spectra, reflection spectra as a function of film thickness, capacitance–voltage characteristics, and performance comparison tables. This material supports the findings presented in the manuscript.

AUTHOR DECLARATIONS
Conflict of Interest

The authors have no conflicts to disclose.

Author Contributions

Leiming Yu: Conceptualization (equal); Data curation (equal); Formal analysis (equal); Funding acquisition (equal); Investigation (equal); Project administration (equal); Resources (equal); Supervision (equal); Writing – review & editing (equal). **Rui Yang:** Data curation (equal); Formal analysis (equal); Writing – original draft (equal). **Xiangdong Duan:** Data curation (equal); Formal analysis (equal). **Zhuo Wu:** Investigation (equal). **Suicai Zhang:** Project administration (equal); Resources (equal); Supervision (equal); Writing – review & editing (equal). **Xiaohui Song:** Conceptualization (equal); Methodology (equal); Project administration (equal). **Yurong Jiang:** Conceptualization (equal); Methodology (equal); Project administration (equal). **Congxin Xia:** Conceptualization (equal); Funding acquisition (equal); Project administration (equal); Resources (equal); Supervision (equal); Writing – review & editing (equal).

DATA AVAILABILITY

The data that support the finding of this study are available within the article and its supplementary material.

REFERENCES

[1] Y. Jiang, X. Dong, L. Sun, T. Liu, F. Qin, C. Xie, P. Jiang, L. Hu, X. Lu, X. Zhou, W. Meng, N. Li, C. J. Brabec, and Y. Zhou, Nat. Energy **7**(4), 352 (2022).

[2] J. Li, Y. Chen, Z. Fan, H. Liu, J. Liu, Z. Tan, S. Cao, K. Sun, Q. Liu, Z. Wang, L. Fang, and D. He, ACS Appl. Mater. Interfaces **17**(13), 19712 (2025).

[3] Z. B. Lu, J. H. Chen, Y. Y. Wu, H. Y. Wen, D. Chi, and S. H. Huang, Appl. Phys. Lett. **127**(9), 093901 (2025).

[4] R. B. Wang, Y. S. Wang, C. Wu, T. S. Zhai, J. C. Yang, B. Q. Sun, S. Duhm, and N. Koch, Adv. Funct. Mater. **30**(4), 1903440 (2020).

[5] H. Liu, Q. M. Liu, J. P. Liu, Y. G. Zhao, Y. J. Yu, Y. An, G. H. Wei, Y. Z. Li, Y. J. Fu, J. S. Li, and D. Y. He, Sol. Energy Mater. Sol. Cells **264**, 112624 (2024).

[6] Z. B. Lu, Y. Zhu, J. M. Chen, G. Z. Hou, H. C. Song, J. Xu, and K. J. Chen, Org. Electron. **108**, 106576 (2022).

[7] T. Gao, Q. Geng, Z. L. Gao, Y. F. Li, L. Chen, and M. C. Li, ACS Appl. Energy Mater. **4**(11), 12543 (2021).

[8] B. B. Chen, X. N. Zhang, Q. Gao, D. H. Yang, J. W. Chen, X. Chang, C. L. Zhang, Y. H. Bai, M. N. Cui, S. F. Wang, H. Li, B. S. Flavel, and J. H. Chen, Adv. Sci. **11**(12), 2306993 (2024).

[9] R. Li, X. Liu, and J. Chen, Exploration **3**(3), 20220027 (2023).

[10] Q. L. Jiang, J. B. Wu, C. Chen, Z. H. Su, Y. Z. Liu, L. Yang, B. C. He, X. Y. Gao, F. L. Gao, and L. F. Lu, Appl. Phys. Lett. **126**(10), 103902 (2025).

[11] Y. Q. Cui, J. Q. Wei, Y. C. Xiong, Q. Y. T. Shang, Q. Y. Liu, L. G. Huang, Y. Zhang, and W. Yu, J. Phys. Chem. C **128**(7), 2767 (2024).

[12] J. He, Y. M. Wan, P. Q. Gao, J. Tang, and J. C. Ye, Adv. Funct. Mater. **28**(34), 1802192 (2018).

[13] L.-M. Yu, T. Chen, N. Feng, R. Wang, T. Sun, Y. Zhou, H. Wang, Y. Yang, and Z.-H. Lu, Sol. RRL **4**(4), 1900513 (2020).

[14] Y. Sun, P. Gao, J. He, S. Zhou, Z. Ying, X. Yang, Y. Xiang, and J. Ye, Nanoscale Res. Lett. **11**(1), 310 (2016).

[15] R. Z. Shen, Z. H. Sun, Y. B. Shi, Y. R. Zhou, W. W. Guo, Y. Q. Zhou, H. Yan, and F. Z. Liu, ACS Nano **15**(4), 6296 (2021).

[16] W. B. Ji, T. Allen, X. B. Yang, G. S. Zeng, S. De Wolf, and A. Javey, ACS Energy Lett. **5**(3), 897 (2020).

[17] H. Lin, M. Yang, X. Ru, G. Wang, S. Yin, F. Peng, C. Hong, M. Qu, J. Lu, L. Fang, C. Han, P. Procel, O. Isabella, P. Gao, Z. Li, and X. Xu, Nat. Energy **8**(8), 789 (2023).

[18] Z. H. Sun, M. Liu, Y. R. Zhou, Q. Wang, Y. Yang, Y. Q. Zhou, and F. Z. Liu, Sol. Energy Mater. Sol. Cells **235**, 111453 (2022).

[19] B. K. Mondal, S. K. Mostaque, M. A. Rashid, A. Kuddus, H. Shirai, and J. Hossain, Superlattices Microstruct. **152**, 106853 (2021).

[20] B. Q. Liang, X. L. Chen, X. F. Wang, H. Z. Yuan, A. X. Sun, Z. Wang, L. Y. Hu, G. F. Hou, Y. Zhao, and X. D. Zhang, J. Mater. Chem. A **13**(4), 2441 (2025).

[21] Z. T. Luo, C. Yang, X. H. Chen, W. H. Ma, S. Y. Li, and K. X. Fu, J. Materiomics **9**(3), 438 (2023).

[22] Z. B. Lu, G. Z. Hou, J. M. Chen, J. Xu, and K. J. Chen, Sol. RRL **5**(8), 2100255 (2021).

[23]J. Y. Zhu, X. Yang, J. Sheng, P. Q. Gao, and J. C. Ye, ACS Appl. Energy Mater. **1**(6), 2874 (2018).

[24]Y. T. Mo, S. H. Xie, T. Y. Huang, R. B. Liao, J. H. Hu, F. S. Chen, W. T. Huang, J. F. Zhang, J. Chen, L. J. Sun, W. L. Wang, and G. Q. Li, Chem. Eng. J. **519**, 164889 (2025).

[25]Z. Sun, Y. He, B. L. Xiong, S. S. Chen, M. Li, Y. L. Zhou, Y. J. Zheng, K. Sun, and C. Yang, Angew. Chem., Int. Ed. **60**(10), 5036 (2021).

[26]Y. X. Cao, H. L. Liu, F. L. Gao, D. Y. Li, L. Xiang, J. W. Gao, P. Gao, Y. Zhang, and S. T. Li, Surf. Interfaces **37**, 102680 (2023).

[27]M. F. Abdelbar, M. El-Kemary, and N. Fukata, Nano Energy **77**, 105163 (2020).

[28]J. H. Chen, Z. B. Lu, X. T. Wang, Y. E. Luo, Y. Ma, G. Lou, D. Chi, and S. H. Huang, Nanomaterials **14**(20), 1630 (2024).

[29]J. He, P. Q. Gao, Z. H. Ling, L. Ding, Z. H. Yang, J. C. Ye, and Y. Cui, ACS Nano **10**(12), 11525 (2016).

[30]A. M. Ali, D. A. Said, M. Khayyat, M. Boustimi, and R. Seoudi, Results Phys. **16**, 102819 (2020).

[31]Y. T. Mo, C. Y. Guo, J. S. Guo, P. X. Liu, X. Wang, Y. F. Cai, J. Y. Chen, X. Deng, W. L. Wang, and G. Q. Li, J. Mater. Chem. A **12**(43), 29562 (2024).

[32]S. Mukherjee, A. Panigrahi, and A. Perumal, ACS Omega **10**(22), 23348 (2025).

[33]T. T. Yang, C. Xu, C. L. Liu, Y. Q. Ye, Z. W. Sun, B. Wang, and Z. Q. Luo, Chem. Eng. J. **429**, 132430 (2022).

[34]X. Fan, W. Nie, H. Tsai, N. Wang, H. Huang, Y. Cheng, R. Wen, L. Ma, F. Yan, and Y. Xia, Adv. Sci. **6**(19), 1900813 (2019).

[35]G. J. Zhang, H. Peng, Q. W. Wei, Z. Zhou, H. X. Wu, J. J. Luo, J. Wang, X. M. Wen, and Y. Yang, ACS Omega **9**(13), 15040 (2024).

[36]D. Won, J. Kim, J. Choi, H. Kim, S. Han, I. Ha, J. Bang, K. K. Kim, Y. Lee, T.-S. Kim, J.-H. Park, C. Y. Kim, and S. H. Ko, Sci. Adv. **8**(23), eabo3209 (2022).

[37]X. S. Rozhkova, A. K. Aimukhanov, B. R. Ilyassov, and A. K. Zeinidenov, Opt. Mater. **131**, 112708 (2022).

[38]M. Zeng, J. Ding, Y. Tian, Y. Zhang, X. Liu, Z. Chen, J. Sun, C. Wu, H. Yin, D. Wei, and H. Fan, Adv. Funct. Mater. **34**(52), 2411390 (2024).

[39]J. Wang, H. Yu, C. Hou, and J. Zhang, ACS Appl. Mater. Interfaces **12**(23), 26543 (2020).

[40]J. Hossain, Q. Liu, T. Miura, K. Kasahara, D. Harada, R. Ishikawa, K. Ueno, and H. Shirai, ACS Appl. Mater. Interfaces **8**(46), 31926 (2016).

[41]Y. Furukawa, J. Phys. Chem. **100**(39), 15644 (1996).

[42]I. Song, N. Y. Park, G. S. Jeong, J. H. Kang, J. H. Seo, and J. Y. Choi, Appl. Surf. Sci. **529**, 147176 (2020).

[43]B. Y. Ouyang, C. W. Chi, F. C. Chen, Q. F. Xi, and Y. Yang, Adv. Funct. Mater. **15**(2), 203 (2005).

[44]J. Ouyang, Q. Xu, C.-W. Chu, Y. Yang, G. Li, and J. Shinar, Polymer **45**(25), 8443 (2004).

[45]G. Zotti, S. Zecchin, G. Schiavon, F. Louwet, L. Groenendaal, X. Crispin, W. Osikowicz, W. Salaneck, and M. Fahlman, Macromolecules **36**(9), 3337 (2003).

[46]S.-M. Kim, C.-H. Kim, Y. Kim, N. Kim, W.-J. Lee, E.-H. Lee, D. Kim, S. Park, K. Lee, J. Rivnay, and M.-H. Yoon, Nat. Commun. **9**(1), 3858 (2018).

[47]Y. H. Kim, C. Sachse, M. L. Machala, C. May, L. Müller-Meskamp, and K. Leo, Adv. Funct. Mater. **21**(6), 1076 (2011).

[48]W. Shen, Y. He, Y. Chen, S. Chen, Z. Chen, C. Liu, H. Cui, S. Liu, L. Liu, G. Cheng, and S. Chen, Laser Photonics Rev. **19**(1), 2400707 (2025).

[49]Y.-J. Lin, F.-M. Yang, and C.-S. Lin, J. Appl. Phys. **102**(10), 103702 (2007).

[50]S. Kondratenko, V. Lysenko, Y. V. Gomeniuk, O. Kondratenko, Y. Kozyrev, O. Selyshchev, V. Dzhagan, and D. R. T. Zahn, ACS Appl. Energy Mater. **2**(8), 5983 (2019).

[51]J. Wang, W. J. Zhou, Q. W. Wei, G. S. Liu, X. B. Yuan, H. Pen, G. J. Zhang, R. F. Wang, C. Wang, and Y. Yang, Adv. Mater. Interfaces **10**(23), 2300187 (2023).

10 January 2026 13:42:30